Scattering of electromagnetic waves by periodic particle arrays

Yu-Lin Xu

ESCG/Orbital Debris Research and Science Operations, Mail Code: JE104, 2224 Bay Area Boulevard, Houston, Texas 77058, USA (yu-lin.xu-1@nasa.gov)

Received February 5, 2013; accepted March 18, 2013;
posted April 3, 2013 (Doc. ID 184890); published May 6, 2013

The generalized multiparticle Mie-solution (GMM) is an extension of the well-known Mie-theory for single homogeneous spheres to the general case of an arbitrary ensemble of variously sized and shaped particles. The present work explores its specific application to periodic structures, starting from one- and two-dimensional regular arrays of identical particles. Emphasis is placed on particle arrays with a truncated periodic structure, i.e., periodic arrays (PAs) with finite overall dimensions. To predict radiative scattering characteristics of a PA with a large number of identical particles within the framework of the GMM, it is sufficient to solve interactive scattering for only one single component particle, unlike the general case where partial scattered fields must be solved for every individual constituent. The total scattering from an array as a whole is simply the convolution of the scattering from a single representative scattering center with the periodic spatial distribution of all replica constituent units, in the terminology of Fourier analysis. Implemented in practical calculations, both computing time and computer memory required by the special version of GMM formulation applicable to PAs are trivial for ordinary desktops and laptops. For illustration, the radiative scattering properties of several regular arrays of identical particles at a fixed spatial orientation are computed and analyzed. Numerical results obtained from the newly developed approach for PAs are compared with those calculated from the general GMM computer codes (that have been available online for about a decade). The two sets of numerical outputs show no significant relative deviations. However, the CPU time required by the specific approach for PAs could drop more than 10,000 times, in comparison with the general approach. In addition, an example PA is also presented, which consists of as large as 10^8 particles and the general solution process is unable to handle.

OCIS codes: (290.4210) Multiple scattering; (290.5825) Scattering theory; (260.1960) Diffraction theory; (050.1755) Computational electromagnetic methods; (050.1940) Diffraction.
http://dx.doi.org/10.1364/JOSAA.30.001053

1. INTRODUCTION

The scattering and absorption of light and other electromagnetic radiation by periodic structures has important applications in a great variety of scientific and technical fields. Authors from diverse research areas have contributed to the theoretical interpretation and analytical representations of the radiative scattering by periodic structures in general or only certain aspects using various theoretical approaches. A substantial portion of recent research is devoted to nanoparticle arrays. It is difficult to exhaust the huge amount of literature on this subject and to digest fully the pith and marrow of every contribution. As a few examples, contributors include Waterman and Pedersen [1]; Psarobas and Stefanov [2]; Yaghjian [3]; Genov *et al.* [4]; Draine and Flatau [5]; and García de Abajo [6]. The work described in Waterman and Pedersen [1] is based on the widely used T-matrix approach that he initiated. The recent work by Draine and Flatau [5] extends the method of discrete-dipole approximation (DDA) to periodic structures. Well known for its superior flexibility, DDA is capable of predicting the scattering properties of a complex and irregular shape [7–9]. A long list of relevant publications can be found in the colloquium by García de Abajo [6].

Multiparticle scattering became rigorously and precisely solvable after the development of the addition theorems for scalar [10] and vector spherical wave functions (VSWFs) [11,12], which provide indispensable mathematical tools to transform wave expansions about a reference center to another one. Following the pioneer work on bisphere scattering by Liang and Lo [13] and Bruning and Lo [14], numerous researchers studied ensemble scattering and made valuable contributions to the development and verification of analytical multiparticle scattering solutions, as well as numerical techniques necessary for practical implementation. For an arbitrary multiparticle configuration illuminated by a monochromatic plane wave with an arbitrary polarization state, a well-established, complete scattering formulation is the generalized multiparticle Mie-solution (GMM) [15–25 and the references therein] with experimental validation [17,20,24]. It is based on the Lorenz–Mie-type multipole superposition method. The solution for the scattering of a monochromatic plane wave is a building block for treating complex beam shapes. The GMM and a set of its public-domain FORTRAN computer codes were developed more than a decade ago and have not been revisited by this author until recently.

Provided all individual proper T-matrices of a number of arbitrarily sized and shaped scattering bodies (i.e., the T-matrices of each of the individual objects when they are isolated and in independent scattering) are known or can be calculated accurately, GMM is capable of predicting reliably the radiative scattering characteristics of an arbitrary external aggregate of these bodies. An arbitrary polarization state of a plane wave can be described in terms of a pair

of orthogonal linear polarization states. All GMM scattering formulations are thus derived from the complete analytical solution to an arbitrary incident linear polarization state. A number of FORTRAN source codes of GMM have been released to the public since 2001 [26]. The public-domain GMM codes solve the individual (or partial) scattered fields for every component particle in respective particle-centered reference systems and place no restriction on either the configuration of an aggregate or the physical and geometrical properties of individual constituent units. However, computer memory and computing time requirements escalate rapidly, and accumulated numerical errors worsen, when the total number and physical sizes of component particles increase. Consequently, the possible maximum number of component particles allowed in an ensemble is limited in practical calculations, which depends on the capacity of available computer power resources and the physical and geometrical properties of individual constituent particles.

To initiate the application of GMM to periodic arrays (PAs), this paper presents an effective and efficient approach to the solution of scattering by one- and two-dimensional regular arrays consisting of a large number of identical particles. Taking advantage of spatial periodicity, the general scattered-field solution process of GMM is drastically simplified. It requires the solution of the partial scattered field for only one single component particle rather than for every constituent unit. Although the simplified solution process is, strictly speaking, derived from the special case of infinite PAs, it opens a useful way to study scattering characteristics of PAs with finite lengths. When the specific solution for PAs is implemented in running computer codes, both computing time and computer memory requirements are always low, insensitive to the total number of particles in a finite PA. For arrays having $\sim 10^6$ wavelength-sized particles, required CPU time is at the level of minutes. Except for the simplification in the scattered-field solution process, all other scattering calculations, such as the amplitude scattering matrix, Mueller matrix, differential and total cross sections of extinction, scattering, absorption, back-scattering and radiation-pressure, as well as electromagnetic fields internal to the individual scattering bodies, remain intact either in formulation or in calculation procedure.

As the basis of the special scattering-field solution process for periodic structures, Section 2 first revisits the most closely related part in the GMM framework, as well as the amplitude scattering matrix, the pivotal quantity in far-field scattering. This brief review attempts to provide a sufficiently clear, conceptual description of the foundation that the present work is based on. For more detailed discussions, readers are referred to relevant GMM publications [15–25]. In preparation for testing the proposed new approach for PAs, numerical results are provided for a few regular particle arrays of finite lengths at a fixed orientation, calculated from the general GMM computer codes that have already been available online for many years. Then, Section 3 presents the specific GMM formulation for PAs, showing how a spatial periodic structure helps to dramatically improve the efficiency of the scattered-field solution process. The specific formulation has been implemented in new FORTRAN codes of GMM, the "PA" series. Numerical results obtained from the PA-type of computer codes are compared favorably with those prepared in Section 2, while the required CPU time shows an incredible reduction. Finally, Section 4 includes conclusions and some discussion on potential future work.

2. REVIEW OF THE SCATTERED-FIELD SOLUTION PROCESS IN GMM

Consider an ensemble of L particles, of finite overall dimensions and illuminated by a linearly polarized monochromatic plane wave of wavelength λ,

$$\mathbf{E}^{\text{inc}} = \mathbf{E}_0 \exp(i\hat{\mathbf{k}} \cdot \mathbf{r} - i\omega t), \tag{1}$$

where $i = \sqrt{-1}$, ω is the circular frequency of the incident plane wave, $\mathbf{r}$ is the position vector, and $\hat{\mathbf{k}}$ is the unit incident vector. The harmonic time dependence $\exp(-i\omega t)$ will be suppressed hereafter. Note the negative sign in the harmonic time term. To be consistent, the first and third types of spherical Bessel functions are used in wave expansions in GMM and the positive sign is used for the imaginary part of the refractive index. Throughout this paper, a boldface indicates the quantity is either a vector or a matrix and ^ designates a unit vector. Also, linear dimensions are always normalized (i.e., multiplied) by the wave number $k = 2\pi/\lambda$. The size, shape, and material compositions of the L individual component particles can all be different. In principle, each of the component particles can be of an arbitrary complex structure itself. In an arbitrarily chosen, primary reference system (PRS), the position vector of every component particle center $l (l = 1, 2, \ldots, L)$ is given by

$$\mathbf{d}^l = \hat{\mathbf{e}}_x X^l + \hat{\mathbf{e}}_y Y^l + \hat{\mathbf{e}}_z Z^l. \tag{2}$$

A lowercase italic superscript denotes the particle identification number. Equivalently, the polar coordinates of particle center l are $(d^l, \vartheta^l, \varphi^l)$, where $d^l = |\mathbf{d}^l|$. In PRS, the incident plane wave propagates in the direction specified by the spherical coordinates $(\vartheta^{\text{inc}}, \varphi^{\text{inc}})$ and the unit incident vector $\hat{\mathbf{k}}$ in Eq. (1) can be written as

$$\hat{\mathbf{k}} = \hat{\mathbf{e}}_x \sin\vartheta^{\text{inc}} \cos\varphi^{\text{inc}} + \hat{\mathbf{e}}_y \sin\vartheta^{\text{inc}} \sin\varphi^{\text{inc}} + \hat{\mathbf{e}}_z \cos\vartheta^{\text{inc}}. \tag{3}$$

When $\vartheta^{\text{inc}} = 0$, $\hat{\mathbf{k}} = \hat{\mathbf{e}}_z$, the incident wave vector points to the positive z direction, which will be referred to as the incident reference system (IRS).

When all $\bar{\mathbf{T}}^l$, the proper T-matrix of every component particle l (i.e., the T-matrix of particle l in single-body scattering when it is isolated), is known or computed with sufficient precision, the radiative scattering characteristics of an ensemble of the particles can be precisely predicted. A key step in solving the multiparticle scattering is to solve scattered and internal fields for all the component particles. This section provides a skeleton review of the general scattered-field solution process in GMM without details. A scattered field varies with the polarization state of the incident plane wave. Since a complex incident polarization state can be described in terms of two orthogonal linear polarizations, to find answers to the scattering of a plane wave with an arbitrary polarization state, it is necessary and sufficient to solve multiparticle scattering for two preferred orthogonal incident linear polarization states. In all GMM computer codes, the two cases of $\beta_p = 0°$ and $90°$ are solved separately, where β_p denotes the linear

polarization angle of the incident plane wave. In IRS, $\vartheta^{\text{inc}} = 0°$, the incident plane wave is x polarized when $\beta_p = 0°$ and y polarized when $\beta_p = 90°$. When $\vartheta^{\text{inc}} \neq 0°$, β_p is defined as the angle between incident electric vector and $\hat{\mathbf{e}}_\theta$, an orthogonal basis unit vector in the polar coordinate system; it is measured in a plane perpendicular to $\hat{\mathbf{k}}$. When the scattering of a plane wave is solved for the two orthogonal linear polarization states, no additional scattered-field calculation is required to treat an elliptical or other complex incident polarization state.

A. Expansion of the Incident Plane Wave

Based on a multipole superposition method of the Lorenz–Mie type, the incident electric field is expanded in terms of VSWFs. In PRS, the expansion of the incident plane wave is expressed as

$$\mathbf{E}^{\text{inc}} = -i \sum_{n=1}^{N_{\max}} \sum_{m=-n}^{n} \sum_{p=1}^{2} E_{mn} p_{mnp} \mathbf{N}_{mnp}^{(1)}(r, \theta, \phi), \tag{4}$$

where (r, θ, ϕ) are spherical coordinates in the PRS, the lowercase italic subscripts m and n specify degree and order of spherical harmonics, the additional lowercase subscript index p denotes transverse magnetic or electric (TM or TE) modes, and $N_{\max}$ is the highest scattering order required to ensure a satisfactory numerical accuracy for the field expansion. Also, the normalization factor used on the right-hand side of Eq. (4) is $E_{mn} = E_0 i^n C_{mn}$ with $E_0 = |\mathbf{E}_0|$ and

$$C_{mn} = \left[\frac{(2n+1)(n-m)!}{n(n+1)(n+m)!}\right]^{1/2}. \tag{5}$$

The VSWFs for incoming waves, $\mathbf{N}_{mnp}^{(1)}$ in Eq. (4), are of the form

$$\begin{aligned}
\mathbf{N}_{mn1}^{(1)} &= \left\{\hat{\mathbf{e}}_r n(n+1) P_n^m(\cos\theta) \frac{j_n(r)}{r} \right. \\
&\quad \left. + [\hat{\mathbf{e}}_\theta \tau_{mn1}(\theta) + \hat{\mathbf{e}}_\phi i \tau_{mn2}(\theta)] \frac{\psi_n'(r)}{r}\right\} \exp(im\phi), \\
\mathbf{N}_{mn2}^{(1)} &= [\hat{\mathbf{e}}_\theta i \tau_{mn2}(\theta) - \hat{\mathbf{e}}_\phi \tau_{mn1}(\theta)] j_n(r) \exp(im\phi),
\end{aligned} \tag{6}$$

where $j_n(r)$ is the spherical Bessel function of the first kind, $\psi_n(r) = r j_n(r)$ is a Riccati–Bessel function, a prime indicates the derivative of a function with respect to its argument, $P_n^m(\cos\theta)$ is the associated Legendre function of the first kind, and the angle-dependent functions, τ_{mnp}, are defined by

$$\begin{aligned}
\tau_{mn1}(\theta) &= \frac{\mathrm{d}}{\mathrm{d}\theta} P_n^m(\cos\theta), \\
\tau_{mn2}(\theta) &= \frac{m}{\sin\theta} P_n^m(\cos\theta).
\end{aligned} \tag{7}$$

The incident field coefficients appearing in Eq. (4) are found through the relation

$$p_{mnp} = \frac{i \int_0^{2\pi} \int_0^{\pi} \exp(i\hat{\mathbf{k}} \cdot \mathbf{r}) \mathbf{E}_0 \cdot \mathbf{N}_{mnp}^{(1)*} \sin\theta \mathrm{d}\theta \mathrm{d}\phi}{E_{mn} \int_0^{2\pi} \int_0^{\pi} |\mathbf{N}_{mnp}^{(1)}|^2 \sin\theta \mathrm{d}\theta \mathrm{d}\phi}. \tag{8}$$

A superscript asterisk stands for complex conjugate. From Eq. (8) follows the explicit expression for incident plane wave with a linear polarization angle β_p,

$$\begin{aligned}
p_{mnp} = (-1)^{m+1} &[\tilde{\tau}_{mnp}(\vartheta^{\text{inc}}) \cos(\varphi^{\text{inc}} - \beta_p) \\
&+ i \tilde{\tau}_{mn3-p}(\vartheta^{\text{inc}}) \sin(\varphi^{\text{inc}} - \beta_p)],
\end{aligned} \tag{9}$$

where $\tilde{\tau}_{mn1}$ and $\tilde{\tau}_{mn2}$ are the angular functions τ_{mnp} modified by C_{mn}, i.e.,

$$\tilde{\tau}_{mnp} = C_{mn} \tau_{mnp}. \tag{10}$$

In IRS, $\vartheta^{\text{inc}} = 0°$, Eq. (9) reduces to

$$\begin{aligned}
p_{mnp} &= 0 \qquad (|m| \neq 1), \\
p_{1np} &= \frac{\sqrt{2n+1}}{2} \exp(-i\beta_p), \\
p_{-1np} &= (-1)^p p_{1np}^*.
\end{aligned} \tag{11}$$

The scattered field of each of the constituent particles in an ensemble is solved in respective particle-centered reference systems, which demand the expansion of the incident plane wave with respect to every particle center. In a translated particle-centered coordinate system, the multipole expansion of the incident plane wave is expressed as

$$\mathbf{E}^{\text{inc},l} = -i \exp(i\hat{\mathbf{k}} \cdot \mathbf{d}^l) \sum_{n=1}^{N_{\max}^l} \sum_{m=-n}^{n} \sum_{p=1}^{2} E_{mn} p_{mnp} \mathbf{N}_{mnp}^{(1)}(r^l, \theta^l, \phi^l), \tag{12}$$

where (r^l, θ^l, ϕ^l) are spherical coordinates in the translated coordinate system centered on particle l. It is worthwhile to emphasize that, with the introduction of the simple incident phase term $\exp(i\hat{\mathbf{k}} \cdot \mathbf{d}^l)$ in Eq. (12), the incident expansion coefficients p_{mnp} in both Eqs. (4) and (12) are identical, independent of the location of particle center.

B. Partial Scattered Fields and their Solution in Fixed-Orientation Scattering

Total scattered field $\mathbf{E}^{\text{sca}}$ from an ensemble of particles is the superposition of the partial scattered fields $\mathbf{E}^{\text{sca},l}$ from all component particles,

$$\mathbf{E}^{\text{sca}} = \sum_{l=1}^{L} \mathbf{E}^{\text{sca},l}. \tag{13}$$

In PRS, the expansion of the total scattered field $\mathbf{E}^{\text{sca}}$ in terms of VSWFs takes the form

$$\mathbf{E}^{\text{sca}} = i \sum_{n=1}^{N_{\max}} \sum_{m=-n}^{n} \sum_{p=1}^{2} E_{mn} a_{mnp} \mathbf{N}_{mnp}^{(3)}(r, \theta, \phi). \tag{14}$$

$\mathbf{N}_{mnp}^{(3)}$ is VSWF for outgoing waves, having the same expressions as Eq. (6) except for the type of the involved spherical Bessel functions,

$$\begin{aligned}
\mathbf{N}_{mn1}^{(3)} &= \left\{\hat{\mathbf{e}}_r n(n+1) P_n^m(\cos\theta) \frac{h_n^{(1)}(r)}{r} \right. \\
&\quad \left. + [\hat{\mathbf{e}}_\theta \tau_{mn1}(\theta) + \hat{\mathbf{e}}_\phi i \tau_{mn2}(\theta)] \frac{\xi_n'(r)}{r}\right\} \exp(im\phi), \\
\mathbf{N}_{mn2}^{(3)} &= [\hat{\mathbf{e}}_\theta i \tau_{mn2}(\theta) - \hat{\mathbf{e}}_\phi \tau_{mn1}(\theta)] h_n^{(1)}(r) \exp(im\phi),
\end{aligned} \tag{15}$$

where $h_n^{(1)}(r)$ represents the spherical Hankel functions of the first kind (also called the spherical Bessel function of the third kind), and $\xi_n(r) = rh_n^{(1)}(r)$ is also a Riccati–Bessel function. Partial scattered fields of every component particle l are expanded in respective particle-centered reference systems,

$$\mathbf{E}^{\mathrm{sca},l} = i\,\exp(i\hat{\mathbf{k}}\cdot\mathbf{d}^l)\sum_{n=1}^{N_{\max}^l}\sum_{m=-n}^{n}\sum_{p=1}^{2}E_{mn}a_{mnp}^l\mathbf{N}_{mnp}^{(3)}(r^l,\theta^l,\phi^l). \tag{16}$$

Exactly the same phase term used in Eq. (12) appears on the right-hand side of the Eq. (16) above. A key step in solving multiparticle scattering is to solve partial interactive scattering coefficients a_{mnp}^l for every component particle by imposing standard boundary conditions at surfaces of the particles [15], given the incident coefficients p_{mnp}. All partial interactive scattering coefficients, a_{mnp}^l, consist of two parts,

$$a_{mnp}^l = \bar{a}_{mnp}^l + \vec{a}_{mnp}^l. \tag{17}$$

The first part $\bar{a}_{mnp}^l$ is the proper scattering coefficients of particle l, which are connected with incident coefficients through the proper T-matrix $\bar{\mathbf{T}}^l$,

$$\bar{a}_{mnp}^l = \sum_{\nu=1}^{N_{\max}^l}\sum_{\mu=-\nu}^{\nu}\sum_{q=1}^{2}\bar{T}_{mnp\mu\nu q}^l p_{\mu\nu q}. \tag{18}$$

The second part on the right-hand side of Eq. (17), $\vec{a}_{mnp}^l$, arises from multiple scattering, i.e., the interaction of particle l with scattered waves from other component particles,

$$\begin{aligned}\vec{a}_{mnp}^l &= \sum_{\nu=1}^{N_{\max}^l}\sum_{\mu=-\nu}^{\nu}\sum_{q=1}^{2}\bar{T}_{mnp\mu\nu q}^l\vec{p}_{\mu\nu q}^l,\\ \vec{p}_{\mu\nu q}^l &= -\sum_{l'=1}^{L}\sum_{n'=1}^{N_{\max}^{l'}}\sum_{m'=-n'}^{n'}\sum_{p'=1}^{2}(1-\delta_{ll'})\\ &\quad\times\exp(i\hat{\mathbf{k}}\cdot\mathbf{d}^{ll'})A_{\mu\nu qm'n'p'}^{ll'}a_{m'n'p'}^{l'}.\end{aligned} \tag{19}$$

In the above Eq. (19), $\delta_{ll'}$ is the Kronecker delta symbol, $\mathbf{d}^{ll'} = \mathbf{d}^{l'} - \mathbf{d}^l$ is the relative position vector extended from particle center l to particle center l', and $A_{\mu\nu qm'n'p'}^{ll'}$ are vector translation coefficients [11,12] characterizing the transformation of the scattered waves from particle l' into incident waves for particle l. Note the notations used in this work for T-matrix elements and vector translation coefficients, such as in Eqs. (18) and (19), are slightly different from those used in earlier publications by this author: $\bar{T}_{mnp\mu\nu q}^l$ and $A_{\mu\nu qm'n'p'}^{ll'}$ replace $\bar{T}_{mn\mu\nu}^{lpq}$ and $A_{\mu\nu m'n'}^{l'lqp'}$.

Addition theorems play a key role in formulating and calculating multiparticle scattering. Explicit expressions and recurrence formulae used in GMM for vector translation coefficients can be found elsewhere [24,27–31], which are based mainly on the work of Cruzan [12]. Cruzan's formulas use Gaunt coefficients [32] and Wigner $3jm$ symbols [33]. The analytical expressions for the vector addition coefficients derived by Cruzan were not considered flawless by several researchers, including this author [28,29]. But after comparing with those derived in alternative ways [18,24,31], clearly, Cruzan's derivation and formulae are correct.

The linear system represented by Eqs. (17)–(19) can be alternatively written as

$$\begin{aligned}&a_{mnp}^l + \sum_{l'=1}^{L}\sum_{n'=1}^{N_{\max}^{l'}}\sum_{m'=-n'}^{n'}\sum_{p'=1}^{2}\sum_{\nu=1}^{N_{\max}^l}\sum_{\mu=-\nu}^{\nu}\sum_{q=1}^{2}(1-\delta_{ll'})\\ &\quad\times\exp(i\hat{\mathbf{k}}\cdot\mathbf{d}^{ll'})\bar{T}_{mnp\mu\nu q}^l A_{\mu\nu qm'n'p'}^{ll'}a_{m'n'p'}^{l'} = \bar{a}_{mnp}^l.\end{aligned} \tag{20}$$

When an individual component particle l is a homogeneous sphere, its proper T-matrix elements $\bar{T}_{mnp\mu\nu q}^l$ are simply the Mie scattering coefficients $\bar{a}_{np}^l$,

$$\bar{T}_{mnp\mu\nu q}^l = \bar{a}_{np}^l\delta_{m\mu}\delta_{n\nu}\delta_{pq}, \tag{21}$$

and for sphere l, Eq. (20) reduces to

$$\begin{aligned}&a_{mnp}^l + \bar{a}_{np}^l\sum_{l'=1}^{L}\sum_{n'=1}^{N_{\max}^{l'}}\sum_{m'=-n'}^{n'}\sum_{p'=1}^{2}(1-\delta_{ll'})\\ &\quad\times\exp(i\hat{\mathbf{k}}\cdot\mathbf{d}^{ll'})A_{mnpm'n'p'}^{ll'}a_{m'n'p'}^{l'} = \bar{a}_{np}^l p_{mnp}.\end{aligned} \tag{22}$$

To solve the linear system for the desired partial interactive scattering coefficients a_{mnp}^l of the L component particles, all GMM public-domain computer codes use BICGSTAB, the bi-conjugate gradient method [34,35].

GMM has another form of linear system for solving the partial interactive scattering coefficients that is based on the T-matrix $\mathbf{T}^{lj}$,

$$a_{mnp}^l = \sum_{j=1}^{L}\sum_{\nu=1}^{N_{\max}^j}\sum_{\mu=-\nu}^{\nu}\sum_{q=1}^{2}\exp(i\hat{\mathbf{k}}\cdot\mathbf{d}^{lj})T_{mnp\mu\nu q}^{lj}p_{\mu\nu q}, \tag{23}$$

where

$$\begin{aligned}T_{mnp\mu\nu q}^{lj} &= j_0(d^{jl})\bar{T}_{mnp\mu\nu q}^l + \sum_{j'=1}^{L}j_0(d^{jj'})\Bigg[(\delta_{jj'}-1)T_{mnp\mu\nu q}^{lj'}\\ &\quad+\sum_{\nu'=1}^{N_{\max}^l}\sum_{\mu'=-\nu'}^{\nu'}\sum_{q'=1}^{2}\sum_{l'=1}^{L}\sum_{n'=1}^{N_{\max}^{l'}}\sum_{m'=-n'}^{n'}\sum_{p'=1}^{2}(\delta_{ll'}-1)\\ &\quad\times\bar{T}_{mnp\mu'\nu'q'}^l A_{\mu'\nu'q'm'n'p'}^{ll'}T_{m'n'p'\mu\nu q}^{l'j'}\Bigg],\end{aligned} \tag{24}$$

with j_0 being the zero-order spherical Bessel function of the first kind. When particle l is a homogeneous sphere, Eq. (24) becomes

$$\begin{aligned}T_{mnp\mu\nu q}^{lj} &= j_0(d^{lj})\bar{a}_{np}^l\delta_{m\mu}\delta_{n\nu}\delta_{pq} + \sum_{j'=1}^{L}j_0(d^{jj'})\\ &\quad\times\Bigg[(\delta_{jj'}-1)T_{mnp\mu\nu q}^{lj'} + \sum_{l'=1}^{L}\sum_{n'=1}^{N_{\max}^{l'}}\sum_{m'=-n'}^{n'}\sum_{p'=1}^{2}(\delta_{ll'}-1)\\ &\quad\times\bar{a}_{np}^l A_{\mu'\nu'q'm'n'p'}^{ll'}T_{m'n'p'\mu\nu q}^{l'j'}\Bigg].\end{aligned} \tag{25}$$

The two linear systems represented by Eqs. (17)–(19) and Eqs. (23) with (24) are equivalent, as regards the solution of the partial scattered fields.

C. Scattered Far-Field and the Amplitude Scattering Matrix

The amplitude scattering matrix that relates scattered amplitudes with those of incident radiation is of pivotal importance, both to the description of far-field scattering and to treat the scattering of a plane wave with a general incident polarization state. The scattering Mueller matrix, which relates scattered and incident Stokes vectors, can be directly calculated from the amplitude scattering matrix [36,37]. What follows is a brief review of the solution and formulation of the 2×2 amplitude scattering matrix in GMM, with emphasis on some subtle points concerning its definition. The derivation of the amplitude matrix in GMM follows the way provided in van der Hulst [36] and Bohren and Huffman [37]. However, it is important to recall that the definition of the amplitude matrix, finally used in the GMM and all its computer codes, is slightly different from the one defined by van der Hulst and Bohren and Huffman, although there is no essential difference in principle. For the matrix adopted in GMM, the concept of "scattering plane" is no longer used, i.e., there is no need to consider incident amplitude components with respect to a "scattering plane."

In far field ($r\to\infty$), the radial component in Eq. (15) vanishes,

$$\xi_n(r)\to(-i)^{n+1}\exp(ir),\qquad \xi_n'(r)\to(-i)^n\exp(ir),\tag{26}$$

and Eq. (15) becomes asymptotically

$$\begin{aligned}\mathbf{N}_{mn1}^{(3)}&=(-i)^n\frac{\exp(ir)}{r}[\hat{\mathbf{e}}_\theta\tau_{mn1}(\theta)+\hat{\mathbf{e}}_\phi i\tau_{mn2}(\theta)]\exp(im\phi),\\ \mathbf{N}_{mn2}^{(3)}&=(-i)^n\frac{\exp(ir)}{r}[\hat{\mathbf{e}}_\theta\tau_{mn2}(\theta)+\hat{\mathbf{e}}_\phi i\tau_{mn1}(\theta)]\exp(im\phi).\end{aligned}\tag{27}$$

Thus, the two scattered far-field transverse components are

$$\begin{aligned}E_\theta^{\mathrm{sca}}(\theta,\phi)&=iE_0\frac{\exp(ir)}{r}\sum_{n=1}^{N_{\max}}\sum_{m=-n}^{n}\sum_{p=1}^{2}a_{mnp}\tilde{\tau}_{mnp}(\theta)\exp(im\phi),\\ E_\phi^{\mathrm{sca}}(\theta,\phi)&=-E_0\frac{\exp(ir)}{r}\sum_{n=1}^{N_{\max}}\sum_{m=-n}^{n}\sum_{p=1}^{2}a_{mnp}\tilde{\tau}_{mn3-p}(\theta)\exp(im\phi).\end{aligned}\tag{28}$$

In GMM, the amplitude scattering matrix for either an individual component particle or an entire ensemble is first solved analytically for an arbitrary linear polarization state of an incident plane wave, which is applicable to either one of a preferred pair of orthogonal linear incident polarization states. Following the convention used by van der Hulst [36] and Bohren and Haffman [37], the derivation is based on the concept of "scattering plane," defined by scattering and incident directions in IRS, in which the incident vector points to the positive z direction. Accordingly, the basic equation used in the derivation of the 2×2 amplitude matrix in GMM is [15–25]

$$\begin{aligned}\begin{pmatrix}E_\parallel^{\mathrm{sca}}\\ E_\perp^{\mathrm{sca}}\end{pmatrix}&=\begin{pmatrix}E_\theta^{\mathrm{sca}}\\ -E_\phi^{\mathrm{sca}}\end{pmatrix}=\frac{\exp(ir)}{-ir}\tilde{\mathbf{S}}\begin{pmatrix}E_\parallel^{\mathrm{inc}}\\ E_\perp^{\mathrm{inc}}\end{pmatrix}\\ &=\frac{\exp(ir)}{-ir}\tilde{\mathbf{S}}\begin{bmatrix}\cos\phi & -\sin\phi\\ \sin\phi & \cos\phi\end{bmatrix}\begin{pmatrix}E_0\cos\beta_p\\ -E_0\sin\beta_p\end{pmatrix}\\ &=\frac{\exp(ir)}{-ir}\begin{bmatrix}\tilde{S}_2 & \tilde{S}_3\\ \tilde{S}_4 & \tilde{S}_1\end{bmatrix}\begin{pmatrix}E_0\cos(\phi-\beta_p)\\ E_0\sin(\phi-\beta_p)\end{pmatrix}.\end{aligned}\tag{29}$$

The four elements of $\tilde{\mathbf{S}}$, which relate scattered and incident amplitudes when the incident plane wave is linearly polarized with an arbitrary linear polarization angle β_p, are obtained for particle l as [15]

$$\begin{aligned}\tilde{S}_2^l(\theta^l,\phi^l)&=\sum_{n=1}^{N_{\max}^l}\sum_{m=0}^{n}\sum_{p=1}^{2}f_m[a_{mnp}^l\exp(i\phi_m)\\ &\quad-(-1)^{m+p}a_{-mnp}^l\exp(-i\phi_m)]\tilde{\tau}_{mnp}(\theta^l),\\ \tilde{S}_3^l(\theta^l,\phi^l)&=i\sum_{n=1}^{N_{\max}^l}\sum_{m=0}^{n}\sum_{p=1}^{2}f_m[a_{mnp}^l\exp(i\phi_m)\\ &\quad+(-1)^{m+p}a_{-mnp}^l\exp(-i\phi_m)]\tilde{\tau}_{mnp}(\theta^l),\\ \tilde{S}_4^l(\theta^l,\phi^l)&=-i\sum_{n=1}^{N_{\max}^l}\sum_{m=0}^{n}\sum_{p=1}^{2}f_m[a_{mnp}^l\exp(i\phi_m)\\ &\quad-(-1)^{m+p}a_{-mnp}^l\exp(-i\phi_m)]\tilde{\tau}_{mn3-p}(\theta^l),\\ \tilde{S}_1^l(\theta^l,\phi^l)&=\sum_{n=1}^{N_{\max}^l}\sum_{m=0}^{n}\sum_{p=1}^{2}f_m[a_{mnp}^l\exp(i\phi_m)\\ &\quad+(-1)^{m+p}a_{-mnp}^l\exp(-i\phi_m)]\tilde{\tau}_{mn3-p}(\theta^l),\end{aligned}\tag{30}$$

where

$$\phi_m=(m-1)\phi^l+\beta_p,\qquad f_m=(1+\delta_{0m})^{-1}.\tag{31}$$

The analytical expressions in Eq. (30) are derived in terms of two incident-amplitude components, which are parallel and perpendicular to the scattering plane and vary with azimuth angle ϕ [15]. The 2×2 ϕ-dependent matrix appearing on the right-hand side of Eq. (29), which governs the variation of the two parallel and perpendicular components of the incident amplitude in different scattering planes, is not included in the matrix $\tilde{\mathbf{S}}$. What is actually used in GMM is slightly different from $\tilde{\mathbf{S}}$, as defined in the following relation [15–25],

$$\begin{pmatrix}E_\theta^{\mathrm{sca}}\\ -E_\phi^{\mathrm{sca}}\end{pmatrix}=\frac{\exp(ir)}{-ir}\mathbf{S}\begin{pmatrix}E_0\cos\beta_p\\ -E_0\sin\beta_p\end{pmatrix}.\tag{32}$$

The equation above is the same as Eq. (29), except for the absorption of the four-element ϕ-dependent matrix into the amplitude matrix,

$$\mathbf{S}=\tilde{\mathbf{S}}\begin{bmatrix}\cos\phi & -\sin\phi\\ \sin\phi & \cos\phi\end{bmatrix}.\tag{33}$$

With the use of $\mathbf{S}$ instead of $\tilde{\mathbf{S}}$, one does not need to refer to "scattering plane" any more. From Eqs. (30) with (31) and (33), it readily follows that

$$S_2^l = \sum_{n=1}^{N_{\max}^l}\sum_{m=0}^{n}\sum_{p=1}^{2} f_m[a_{mnp}^l \tilde{\tau}_{mnp}\ \exp(im\phi^l)\exp(i\beta_p) + a_{-mnp}^l \tilde{\tau}_{-mnp}\ \exp(-im\phi^l)\exp(-i\beta_p)],$$

$$S_3^l = i\sum_{n=1}^{N_{\max}^l}\sum_{m=0}^{n}\sum_{p=1}^{2} f_m[a_{mnp}^l \tilde{\tau}_{mnp}\ \exp(im\phi^l)\exp(i\beta_p) - a_{-mnp}^l \tilde{\tau}_{-mnp}\ \exp(-im\phi^l)\exp(-i\beta_p)],$$

$$S_4^l = -i\sum_{n=1}^{N_{\max}^l}\sum_{m=0}^{n}\sum_{p=1}^{2} f_m[a_{mnp}^l \tilde{\tau}_{mn3-p}\ \exp(im\phi^l)\exp(i\beta_p) + a_{-mnp}^l \tilde{\tau}_{-mn3-p}\ \exp(-im\phi^l)\exp(-i\beta_p)],$$

$$S_1^l = \sum_{n=1}^{N_{\max}^l}\sum_{m=0}^{n}\sum_{p=1}^{2} f_m[a_{mnp}^l \tilde{\tau}_{mn3-p}\ \exp(im\phi^l)\exp(i\beta_p) - a_{-mnp}^l \tilde{\tau}_{-mn3-p}\ \exp(-im\phi^l)\exp(-i\beta_p)]. \quad (34)$$

It is apparent that only the two elements S_2 and S_4 of the amplitude matrix are obtained when $\beta_p = 0°$ and, similarly, only S_3 and S_1 are evaluated when $\beta_p = 90°$. Written explicitly in terms of the two orthogonal linear incident polarizations of $\beta_p = 0°$ and 90° that are normally used in scattering calculations, Eq. (34) becomes [21–25]

$$S_2^l = \sum_{n=1}^{N_{\max}^l}\sum_{m=-n}^{n}\sum_{p=1}^{2} a_{mnp}^{l(0°)} \tilde{\tau}_{mnp}(\theta^l)\exp(im\phi^l),$$

$$S_3^l = -\sum_{n=1}^{N_{\max}^l}\sum_{m=-n}^{n}\sum_{p=1}^{2} a_{mnp}^{l(90°)} \tilde{\tau}_{mnp}(\theta^l)\exp(im\phi^l),$$

$$S_4^l = -i\sum_{n=1}^{N_{\max}^l}\sum_{m=-n}^{n}\sum_{p=1}^{2} a_{mnp}^{l(0°)} \tilde{\tau}_{mn3-p}(\theta^l)\exp(im\phi^l),$$

$$S_1^l = i\sum_{n=1}^{N_{\max}^l}\sum_{m=-n}^{n}\sum_{p=1}^{2} a_{mnp}^{l(90°)} \tilde{\tau}_{mn3-p}(\theta^l)\exp(im\phi^l). \quad (35)$$

The superscripts (0°) and (90°) of the scattering coefficients indicate the associated linear incident polarization angle. Note that Eqs. (34) and (35) are general, applicable to a general incident direction. The total scattering far-field coefficients in Eq. (14), a_{mnp}, and the total amplitude scattering matrix of an ensemble of particles are, respectively,

$$a_{mnp} = \sum_{l=1}^{L} \exp[i\mathbf{d}^l \cdot (\hat{\mathbf{k}} - \hat{\mathbf{r}})] a_{mnp}^l,$$

$$\mathbf{S} = \sum_{l=1}^{L} \exp[i\mathbf{d}^l \cdot (\hat{\mathbf{k}} - \hat{\mathbf{r}})] \mathbf{S}^l. \quad (36)$$

Expressed in terms of the total scattering coefficients, a_{mnp}, the four elements of the total amplitude matrix are of the same form as Eq. (35) but with all superscript l removed.

D. Numerical Examples: One- and Two-Dimensional Regular Particle Arrays

Table 1 lists five examples for regular arrays of identical particles. These five finite PAs include two linear chains and three square arrays, in which all component particles have the same refractive index of (1.6, 0.1). IRS is used in all the scattering calculations. Labeled with the ID of "L1," the first example is a linear chain of 3001 identical prolate spheroids, illuminated by a monochromatic plane wave of wavelength 31.416 mm. An individual spheroid is of aspect ratio 0.5 (i.e., the minor-to-major axis ratio). A sphere of diameter 1 mm has an equivalent volume. The orientation of the spheroids is such that their major (rotational) axes are parallel to the z axis, i.e., aligned along the incident direction. All particle centers fall on the x axis, spaced at equal 1 mm intervals. The second example of "L2" is a linear chain of identical homogeneous spheres of 1 mm diameter. The wavelength of the incident plane wave is 3.1416 mm and each individual sphere has a size parameter of 1.0. All sphere centers are on the x axis, spaced equally 1 mm apart, i.e., neighboring spheres are in contact. The third example of "S1" is a 101×101 square array of identical prolate spheroids with rows parallel to the x axis and columns parallel to the y axis. An individual spheroid has exactly the same geometrical and physical parameter and spatial orientation as the first example of the linear array L1. The wavelength of the incident plane wave is 31.416 mm. All spheroid centers are in the x–y plane, spaced equally 1 mm apart in each row or column. The fourth and fifth examples of "S2" and "S3" are similar 101×101 and 201×201 square arrays. For both S2 and S3, each individual component particle is a sphere of 1 mm diameter and the incident wavelength is 3.1416 mm.

Numerical solutions shown are for a single fixed orientation, obtained from the GMM computer codes currently available online. Table 2 shows the computer memory and CPU time required for the calculations using an 8-Core 2.4GHz DELL PRECISION T7500 desktop computer. Calculations for the two arrays of L1 and S1 use the public-domain GMM code "gmm03s.f" and L2, S2, and S3 use "gmm01s.f". Table 3 presents numerical results of total cross sections for extinction, absorption, scattering, back-scattering, and radiation pressure, which are the average over the two orthogonal linear polarization states of the incident plane wave. This means the total cross sections shown in Table 3 are for an unpolarized incident plane wave.

Outputs of the scattering calculations include the amplitude scattering matrix and thus, the Mueller matrix. Results of 4 out of the 16 Mueller matrix elements are presented in Figs. 1–4

Table 1. Five Examples for Regular Arrays of Identical Particles

Array ID	Array Type	No. of Particles	Individual-Particle Parameter		
			Shape	Size Parameter	Referactive Index
L1	Linear	3001	Prolate spheroid (1:2)	0.1 (volume equiv.)	$1.6 + i0.1$
L2	Linear	3001	Sphere	1.0	$1.6 + i0.1$
S1	Square	101×101	Prolate spheroid (1:2)	0.1 (volume equiv.)	$1.6 + i0.1$
S2	Square	101×101	Sphere	1.0	$1.6 + i0.1$
S3	Square	201×201	Sphere	1.0	$1.6 + i0.1$

Table 2. Computer Memory and CPU Time Required in the Scattering Calculations on an 8-Core 2.4 GHz DELL PRECISION T7500 Desktop Computer for the Regular Arrays of Identical Particles Listed in Table 1 (When Using the General GMM Computer Codes that are Currently Available Online)

Array-ID	L1	L2	S1	S2	S3
CPU (min)	38.2	101.8	450.9	3088.3	52135.3
Memory (Gb)	1.3	0.22	3.7	0.57	2.1

Table 3. Total Cross Sections for Extinction, Absorption, Scattering, Backscattering, and Radiation Pressure (mm^2) Calculated from the General GMM Computer Codes "gmm01s.f" or "gmm03s.f" for the Regular Arrays of Identical Particles Listed in Table 1

Array-ID	Cext	Cabs	Csca	Cbak	Cpr
L1	44.966	43.544	1.4222	329.98	44.957
L2	1711.8	586.55	1125.3	1.3734e6	1369.9
S1	239.82	174.12	65.702	4467.8	239.16
S2	5204.1	1599.5	3605.8	9.0231e6	2993.0
S3	20604	6309.1	14292	1.4099e8	1.1805e4

for the linear array L1, showing, respectively, the variation of S_{11}, S_{22}/S_{11}, S_{33}/S_{11}, and S_{44}/S_{11}, with scattering angle θ and azimuth angle ϕ. Each of the figures have four panels. The left two panels are for the forward hemisphere of $0° \le \theta \le 90°$ (with $\theta = 0°$ for the exact forward scattering direction) and the right two panels are for the backward hemisphere of $90° \le \theta \le 180°$, with $\theta = 180°$ being the exact backward scattering direction. The lower two panels present the same data shown in the upper two panels in an alternative way. Because of limited space, the other 12 Mueller matrix elements of L1 and the Mueller matrices of other arrays are not shown.

E. Scattering Characteristics of an Individual Component Particle and the Edge Effect

The total scattering from an array of particles includes contributions from every individual constituent particle. Shown in Fig. 5 are the individual extinction and absorption cross sections of the 3001 spheroids in the linear array of L1. The particle identification numbers shown in Fig. 5 reflect the locations of the component spheroids in the linear array from end-to-end.

We see from Fig. 5 that the individual extinction and absorption cross sections are the same for the majority of the 3001 particles, with the exception of several particles near both ends. A multiparticle scattering formulation must take into account the interaction effect, i.e., the response of an individual component particle to the scattered radiation from other component particles. For the PAs of identical particles under consideration, the proper scattering is identical for all component particles. The interactive scattering of an individual component particle depends on its location in an array. As Eq. (19) indicates, given the physical and geometrical properties of an individual particle, its interactive scattering is determined by the local spatial distribution of other component particles around the particle with respect to its center. The change in scattering behavior of the particles near edges, in comparison with inner ones, is caused by a change in the

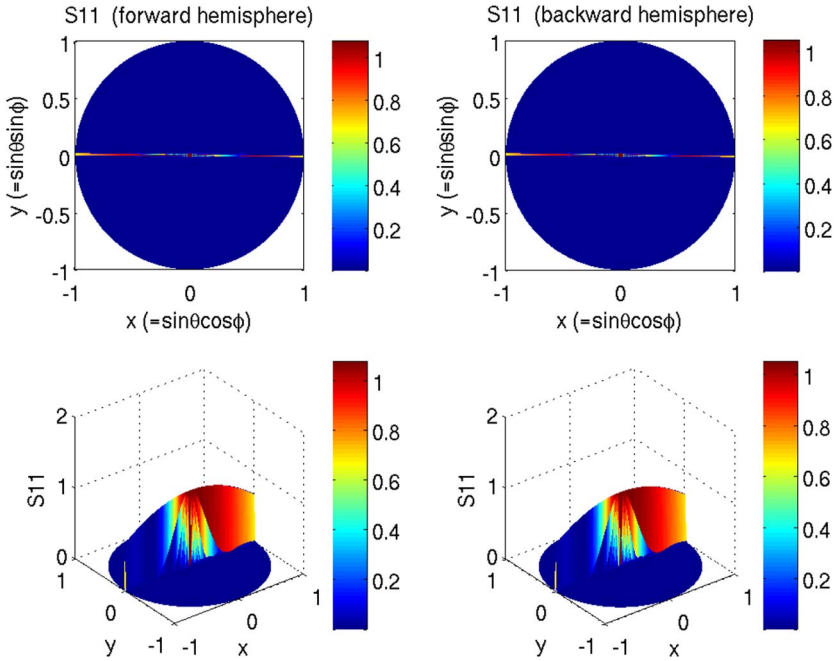

Fig. 1. Dependence of the Mueller matrix element S_{11} on scattering angle θ and azimuth angle φ (shown as variation with $x = \sin\theta\cos\varphi$ and $y = \sin\theta\sin\varphi$) for the particle array L1 (see Table 1), which is a linear chain of 3001 identical prolate spheroids of refractive index (1.6, 0.1). The incident plane wave is of wavelength 31.416 mm, propagating in the positive z direction. An individual spheroid has an aspect ratio (i.e., the minor-to-major axis ratio) of 0.5. Its volume-equivalent sphere diameter is 1 mm. Geometrical centers of the spheroids are aligned along the x axis, equally spaced by 1 mm. The major (rotational) axes of the spheroids are parallel to the z axis. In the four panels, the left two are for the forward hemisphere of $0° \le \theta \le 90°$ (with $\theta = 0°$ being the exact forward scattering direction) and the right two are for the backward hemisphere of $90° \le \theta \le 180°$ (with $\theta = 180°$ being the exact backward scattering direction). The lower two panels are equivalent to the upper two, simply presenting the same data in an alternative way.

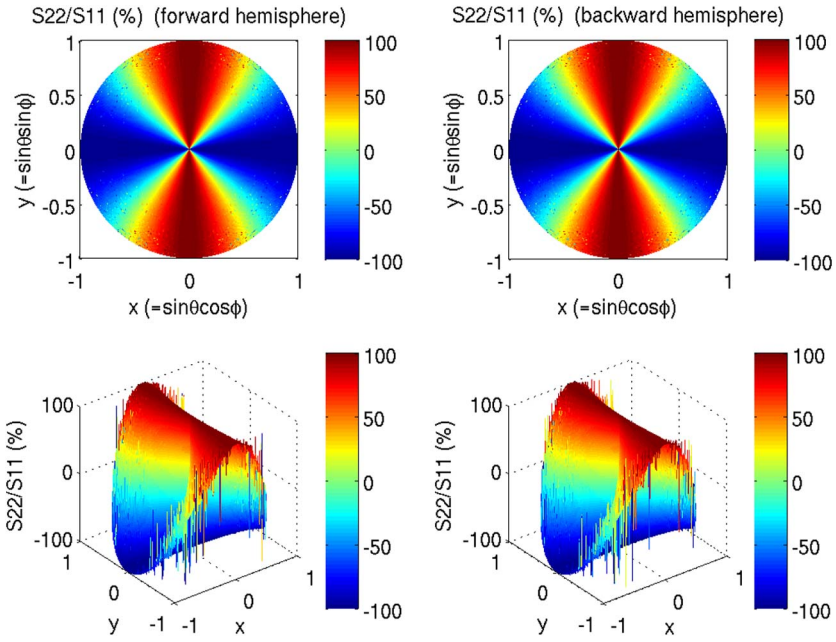

Fig. 2. Dependence of the Mueller matrix element ratio S_{22}/S_{11} on scattering angle θ and azimuth angle φ (shown as variation with $x = \sin\theta\cos\varphi$ and $y = \sin\theta\sin\varphi$) for the same linear spheroid array of L1 as shown in Fig. 1.

spatial distribution pattern of other component particles around them, referred to as an "edge effect." As the total particle number in an array increases, the edge effect will gradually weaken and fade away.

3. APPLICATION OF GMM TO PERIODIC PARTICLE ARRAYS

The general GMM solution process, briefly reviewed in the last section, is devised for an arbitrary configuration of noninter-secting scattering bodies with mixed shapes, sizes, material compositions, and structures. In practical calculations using the general GMM codes available online, required computer memory and computing time are determined by the maximum size and total number of component scattering units. Ceilings exist for the maximum total number and the largest size of constituent scattering bodies allowed in an ensemble. When applied to periodic structures, the favorable spatial periodicity helps to remarkably simplify the scattered-field solution process and to relax the limitations.

This section presents a special version of the GMM formulation for one- and two-dimensional PAs of identical particles, which has been implemented in a new PA-series of GMM codes. The PA-type codes do not demand excessive computer

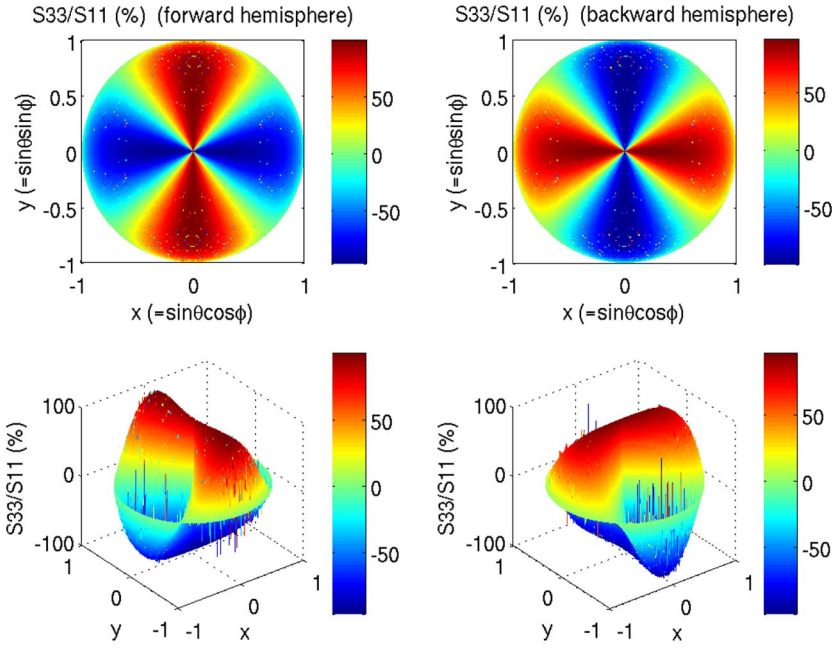

Fig. 3. Dependence of the Mueller matrix element ratio S_{33}/S_{11} on scattering angle θ and azimuth angle φ (shown as variation with $x = \sin\theta\cos\varphi$ and $y = \sin\theta\sin\varphi$) for the same linear spheroid array of L1 as shown in Fig. 1.

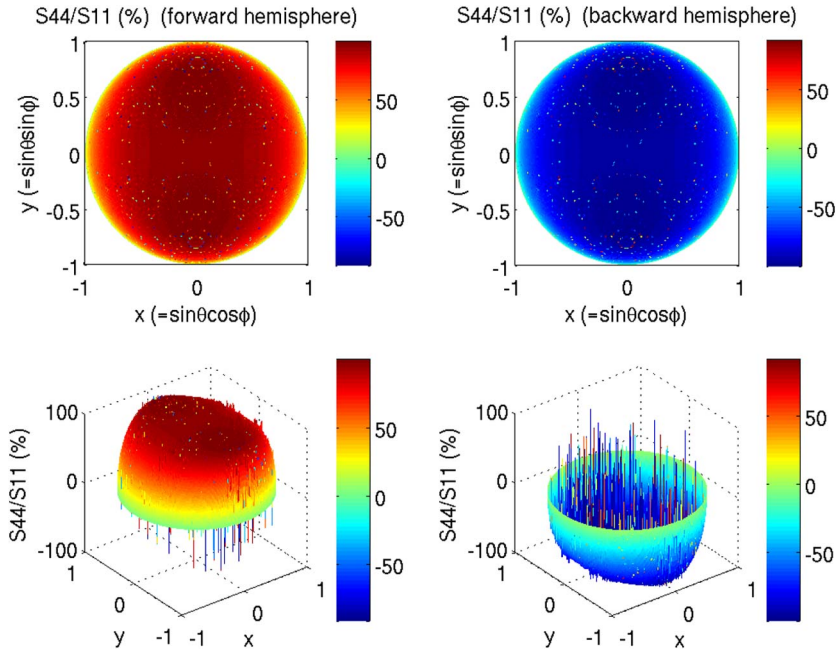

Fig. 4. Dependence of the Mueller matrix element ratio S_{44}/S_{11} on scattering angle θ and azimuth angle φ (shown as variation with $x = \sin\theta\cos\varphi$ and $y = \sin\theta\sin\varphi$) for the same linear spheroid array of L1 as shown in Fig. 1.

memory or computing time and thus, are able to handle PAs with a huge number of particles. To demonstrate, a regular array consisting of as large as 10^8 particles is calculated. Numerical solutions, obtained from the special GMM formulation for the same particle arrays listed in Table 1, are compared with those calculated from the general GMM codes presented in the previous section. While numerical results are similar, there are tremendous savings in computing time. It is also evident that, since a substantial part of computations are bypassed, numerical errors otherwise accumulated in relevant computations are circumvented.

A. Infinite-Dimension Periodic Arrays

As the GMM general formulation clearly shows, despite a constant phase shift, the scattered fields from two identical constituent units will be exactly the same when surrounding component units for the two have exactly the same physical and geometrical properties and the same local spatial distribution. In this regard, since infinite PAs of identical particles have no edges, the partial scattered fields from all individual component particles are identical (when incidence phase shift terms about different particle centers are excluded, as in the GMM formulation). This is to say, for infinite arrays, partial scattering coefficients a^l_{mnp} are identical for all component particles; in Eq. (19), the interactive scattering part of any individual component particle l reduces to

$$\vec{a}^l_{mnp} = \sum_{\nu=1}^{N^l_{\max}} \sum_{\mu=-\nu}^{\nu} \sum_{q=1}^{2} \bar{T}^l_{mnp\mu\nu q} \vec{p}^l_{\mu\nu q},$$

$$\vec{p}^l_{\mu\nu q} = -\sum_{n'=1}^{N^l_{\max}} \sum_{m'=-n'}^{n'} \sum_{p'=1}^{2} C^l_{\mu\nu qm'n'p'} a^l_{m'n'p'},$$

$$C^l_{\mu\nu qm'n'p'} = \sum_{l'} (1-\delta_{ll'}) \exp(i\hat{\mathbf{k}}\cdot\mathbf{d}^{ll'}) A^{ll'}_{\mu\nu qm'n'p'}. \tag{37}$$

This leads to the following linear system, which involves partial scattering coefficients of only one single component particle,

$$a^l_{mnp} + \sum_{n'=1}^{N^l_{\max}} \sum_{m'=-n'}^{n'} \sum_{p'=1}^{2} \sum_{\nu=1}^{N^l_{\max}} \sum_{\mu=-\nu}^{\nu} \sum_{q=1}^{2} \bar{T}^l_{mnp\mu\nu q} \times C^l_{\mu\nu qm'n'p'} a^l_{m'n'p'} = \bar{a}^l_{mnp}. \tag{38}$$

The crucial difference of the above Eqs. (37) and (38) from Eqs. (19) and (20) is that all $a^{l'}_{m'n'p'}$ (with $l' = 1, 2, \ldots, L$) in Eqs. (19) and (20) are replaced by $a^l_{m'n'p'}$ of a single component particle l. As a result, the C-coefficients are emerged in Eqs. (37) and (38), which are irrelevant to the intrinsic properties of the component particles in a PA and completely determined by the inherent geometrical structure of the

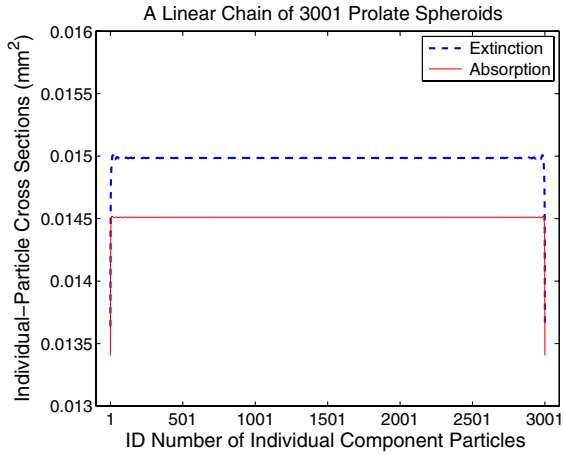

Fig. 5. Extinction and absorption cross sections of the 3001 individual prolate spheroids in the linear array L1, which are identical for the majority of the component particles except for a few at both ends due to the edge effect.

component-particle centers. The C-coefficients can thus be evaluated by summing over only the vector translation coefficients (with appropriate incident phase terms) of all particles l' without involving scattering coefficients. For PAs of identical spheres, it is further simplified,

$$a^l_{mnp} + \bar{a}^l_{np} \sum_{n'=1}^{N^l_{\max}} \sum_{m'=-n'}^{n'} \sum_{p'=1}^{2} C^l_{mnpm'n'p'} a^l_{m'n'p'} = \bar{a}^l_{np} p_{mnp}. \quad (39)$$

The number of unknowns to be solved in the above linear systems is the possible minimum that one can assume for this type, which only depends on the intrinsic properties of an individual particle.

To solve the above linear system for the scattered field of an individual particle in an infinite PA, the calculation of the C-coefficients does not need to include an infinite number of component particle centers. The reason for this is very simple. Numerical values of vector translation coefficients drop steeply as translation distance increases, implying the values of the C-coefficients are determined merely by the component particle centers within a certain distance from particle l. In other words, all component particles sufficiently far from particle l have a negligible contribution, as if they did not exist. The largest translation distance needed to ensure a satisfactory accuracy of numerical solutions can be determined easily in practical calculations by setting an error tolerance, say, 10^{-12} or other small value, as desired. When evaluating a C-coefficients, the vector translation coefficients for the component particle center nearest to particle l are calculated first and then gradually stretched out until the relative change in its value is within the preferred tolerance, as implemented in the new PA-type computer codes of GMM.

As a demonstration, the scattered field of an individual component spheroid in an infinite array of identical prolate spheroids is calculated. The individual prolate spheroid has a refractive index (1.6, 0.1) and an aspect ratio of 0.5, having a volume-equivalent sphere diameter of 1 mm. The prolate spheroid's major axes are all parallel to the z axis. All particle centers are in the x–y plane, equally spaced by 10 mm in the x direction and 1 mm in the y direction. The incident plane wave of wavelength 31.416 mm propagates in the positive z direction. Shown in Fig. 6 is the variation of Stokes parameters I and Q with scattering and azimuth angles when the incident plane wave is linearly x polarized. Similarly, Fig. 7 shows Stokes parameters of U and V when the incident wave is right-circularly polarized. In solving the partial scattered field of an individual component spheroid when the error tolerance is set to 10^{-12}, it is necessary to include $\sim 10^5$ particle centers.

B. Periodic Particle Arrays of Finite Lengths

In practice, arrays with finite dimensions are meaningful and of interest. Based on Eqs. (36)–(38), the total scattered far-field and the total amplitude matrix of a PA consisting of L identical particles can be written approximately as

$$a_{mnp} = a^l_{mnp} \sum_{j=1}^{L} \exp[i\mathbf{d}^j \cdot (\hat{\mathbf{k}} - \hat{\mathbf{r}})],$$
$$\mathbf{S} = \mathbf{S}^l \sum_{j=1}^{L} \exp[i\mathbf{d}^j \cdot (\hat{\mathbf{k}} - \hat{\mathbf{r}})]. \quad (40)$$

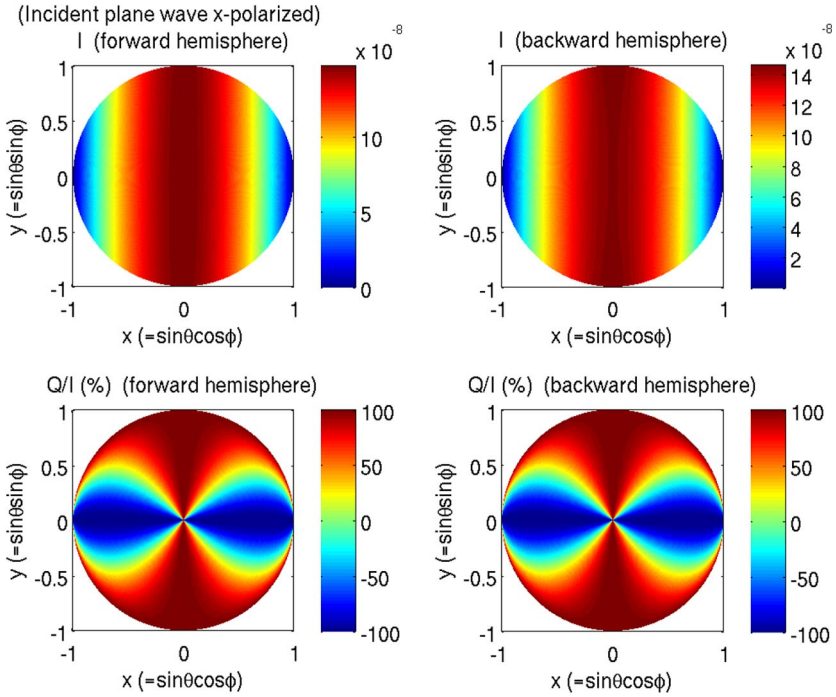

Fig. 6. Dependence of the Stokes parameters I and Q on scattering angle θ and azimuth angle φ (shown as variation with $x = \sin\theta\cos\varphi$ and $y = \sin\theta\sin\varphi$) for an individual spheroid in an infinite array of identical prolate spheroids of refractive index (1.6, 0.1). The incident plane wave of wavelength 31.416 mm is x polarized, propagating in the positive z direction. An individual spheroid has an aspect ratio of 0.5. Its volume-equivalent sphere diameter is 1 mm. The major axes of the spheroids are parallel to the z axis. All particle centers are in the x–y plane, equally spaced by 10 mm in the x direction and 1 mm in the y direction.

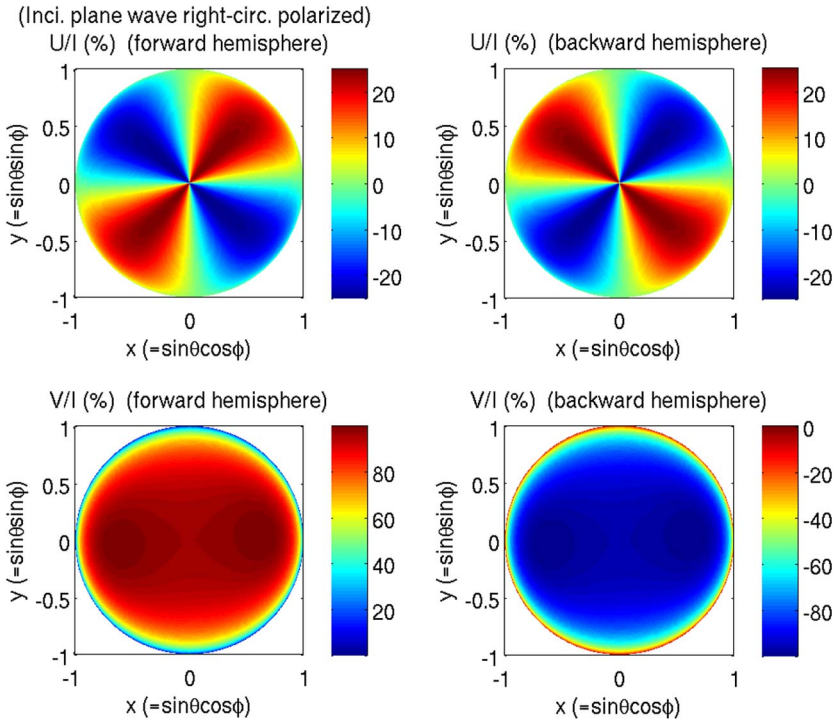

Fig. 7. Same as Fig. 6 but for the Stokes parameters U and V when the incident plane wave is right-circularly polarized.

Note the important differences between Eq. (36) and Eq. (40). As discussed in the last subsection, the partial scattering coefficients a^l_{mnp} are identical in a PA for all replica component particles (with $l = 1, 2, \ldots, L$). Therefore, a^j_{mnp} (with $j = 1, 2, \ldots, L$) in Eq. (36) can all be replaced by a^l_{mnp} of any single component particle l in Eq. (40) and taken out from the summation over the component particles. The total incident and scattered phase term on the right-hand side of the two equations in Eq. (40) involves only incident direction and the geometrical structure of an array and is independent of the partial scattering coefficients of the component particles. Recall that a displacement of an array of particles in PRS, or the PRS itself, causes only a constant phase shift and will not affect any scattering solutions under study.

For one-dimensional periodic particle arrays, it follows from Eqs. (2) and (3) that

$$\mathbf{d}^j \cdot (\hat{\mathbf{k}} - \hat{\mathbf{r}}) = d^j[\cos\eta^j(\vartheta^{\text{inc}}, \varphi^{\text{inc}}) - \cos\eta^j(\theta, \phi)],$$
$$\cos\eta^j(\beta, \alpha) = \sin\beta \sin\vartheta^j \cos(\alpha - \varphi^j) + \cos\beta\cos\vartheta^j. \quad (41)$$

The phase terms have two parts. The first part is an incident phase shift and the second part is a scattered phase term that varies with scattered direction. In Eq. (41), (ϑ^j, φ^j) defines the spatial orientation of the axis of a linear chain, on which all particle centers are located. Since (ϑ^j, φ^j) is independent of the location of a component particle center, $(\vartheta^{\text{lin}}, \varphi^{\text{lin}})$ and $\cos\eta^{\text{lin}}$ can be used to replace (ϑ^j, φ^j) and $\cos\eta^j$ for all replica particles. It is straightforward to show that, for a linear PA of particles,

$$\sum_{j=1}^{L} \exp[i\mathbf{d}^j \cdot (\hat{\mathbf{k}} - \hat{\mathbf{r}})] = \frac{\sin(L \cdot \Delta d \cdot \Phi^{\text{lin}}/2)}{\sin(\Delta d \cdot \Phi^{\text{lin}}/2)},$$
$$\Phi^{\text{lin}} = \cos\eta^{\text{lin}}(\vartheta^{\text{inc}}, \varphi^{\text{inc}}) - \cos\eta^{\text{lin}}(\theta, \phi), \quad (42)$$

where Δd is the separation distance between a pair of adjacent component particle centers. For the case of normal incidence in IRS, when the axis of a linear chain is parallel to the x axis, Eq. (42) becomes much simpler,

$$\sum_{j=1}^{L} \exp[i\mathbf{d}^j \cdot (\hat{\mathbf{k}} - \hat{\mathbf{r}})] = \frac{\sin(L \cdot \Delta x \cdot \sin\theta\cos\phi/2)}{\sin(\Delta x \cdot \sin\theta\cos\phi/2)}. \quad (43)$$

For a rectangular array of $L = N^{\text{row}} \cdot N^{\text{col}}$ identical particles, it can be shown that

$$\sum_{j=1}^{L} \exp[i\mathbf{d}^j \cdot (\hat{\mathbf{k}} - \hat{\mathbf{r}})] = \frac{\sin(N^{\text{row}} \cdot \Delta d^{\text{row}} \cdot \Phi^{\text{row}}/2)}{\sin(\Delta d^{\text{row}} \cdot \Phi^{\text{row}}/2)} \cdot \frac{\sin(N^{\text{col}} \cdot \Delta d^{\text{col}} \cdot \Phi^{\text{col}}/2)}{\sin(\Delta d^{\text{col}} \cdot \Phi^{\text{col}}/2)},$$
$$\Phi^{\text{row}} = \cos\eta^{\text{row}}(\vartheta^{\text{inc}}, \varphi^{\text{inc}}) - \cos\eta^{\text{row}}(\theta, \phi),$$
$$\Phi^{\text{col}} = \cos\eta^{\text{col}}(\vartheta^{\text{inc}}, \varphi^{\text{inc}}) - \cos\eta^{\text{col}}(\theta, \phi). \quad (44)$$

Here, $\cos\eta^{\text{row}}$ and $\cos\eta^{\text{col}}$ are associated with $(\vartheta^{\text{row}}, \varphi^{\text{row}})$ and $(\vartheta^{\text{col}}, \varphi^{\text{col}})$ that define, respectively, the orientation of row and column, whereas Δd^{row} and Δd^{col} are the separation distance between a pair of adjacent particles in each row or column. At normal incidence in IRS, when all the $L = Nx \cdot Ny$ particle centers are in the x–y plane with rows parallel to the x axis and columns parallel to the y axis, Eq. (44) reduces to

$$\sum_{j=1}^{L}\exp[i\mathbf{d}^j\cdot(\hat{\mathbf{k}}-\hat{\mathbf{r}})]=\frac{\sin(Nx\cdot\Delta x\cdot\sin\theta\cos\phi/2)}{\sin(\Delta x\cdot\sin\theta\cos\phi/2)}\cdot\frac{\sin(Ny\cdot\Delta y\cdot\sin\theta\sin\phi/2)}{\sin(\Delta y\cdot\sin\theta\sin\phi/2)}. \quad (45)$$

With the use of the simple results shown in Eqs. (42)–(45), an evaluation of the total incident and scattered phase terms bypasses the computation of the phase shift for an individual particle. These equations, especially Eqs. (43) and (45), are reminiscent of the analogous formulas for the Fraunhofer diffraction of light concerning a large number of apertures. In fact, the phase terms discussed above are nothing else but the Fourier transform of comb functions that represent the spatial distribution of particle centers in a linear chain or a rectangular array. Since a displacement of a scattering center causes only a phase shift term, the angular distribution of the scattered radiation from a regular particle array is simply the convolution of the scattered pattern of a single component particle with the comb functions, consistent with Fourier analysis. Being beyond the scope of this paper, it will not be discussed further.

C. Numerical Results: Comparison with Those Obtained from General GMM Codes

Numerical results obtained from the PA-type FORTRAN codes are shown below for the same particle arrays listed in Table 1. The nonspherical particle arrays L1 and S1 are calculated using "gmm03_PA.f" and the sphere arrays L2, S2, and S3 use "gmm01_PA.f". Presented in Table 4 are total cross-sections for extinction, absorption, scattering, back-scattering and radiation pressure, the same outputs as given in Table 3. Table 5 lists relative deviations in the calculated cross sections, using the corresponding results shown in Table 3 as benchmarks. We see the relative deviations are larger for the three square arrays S1, S2, and S3, compared to those for the two linear chains L1 and L2. One reason is that the ratio of overall dimension to the size of an individual component particle is much smaller for the square arrays. Also, the larger the size parameter of an individual particle, the higher the scattering order required and the larger the numerical errors that will be accumulated in the scattering calculations. Results from these and other similar comparisons suggest that the larger the total number of components in a particle array, the weaker the edge effect and the lower the relative deviations. This is evident from the results for the square arrays S2 and S3. Note that every aspect is the same for the two arrays, except that the total particle number of S3 is four times larger than S2. Nevertheless, calculating large particle arrays through the general solution procedure may demand an unacceptably long computing time, even when sufficient computer memory is available. In contrast, both CPU and computer memory will not be an issue for periodic particle arrays when using the special PA-type codes, which do not increase appreciably when the total number of component particles increases.

Table 4. Total Cross Sections (mm^2) Calculated from the Newly Developed GMM Computer Codes for Periodic Structures ("gmm01_PA.f" or "gmm03_PA.f") for the Regular Arrays of Identical Particles Listed in Table 1

Array-ID	Cext	Cabs	Csca	Cbak	Cpr
L1	44.980	43.555	1.4246	330.03	44.971
L2	1712.1	586.58	1125.6	1.3735e6	1370.1
S1	246.11	177.11	68.996	4329.1	245.36
S2	5414.0	1657.5	3756.6	9.9586e6	3108.9
S3	20752	6483.1	14269	1.5086e8	1.1675e4

Table 5. Relative Deviations of the Total Cross Sections Calculated from the Newly Developed GMM Codes "gmm01_PA.f" or "gmm03_PA.f" Using the Results Shown in Table 3 as a Benchmark

Array-ID	Cext	Cabs	Csca	Cbak	Cpr
L1	3.1e−4	2.5e−4	1.7e−4	1.5e−4	3.1e−4
L2	1.8e−4	5.1e−5	2.7e−4	7.3e−5	1.4e−4
S1	0.026	0.017	0.048	0.032	0.025
S2	0.039	0.035	0.040	0.094	0.037
S3	0.0072	0.028	0.0016	0.070	0.011

Table 6 shows the CPU time and computer memory required on an 8-Core 2.4GHz DELL PRECISION T7500 desktop computer using PA-type codes to calculate the example regular arrays listed in Table 1. Table 7 compares the required CPU and computer memory reported in Table 6 with those required correspondingly by the general solution process of GMM as listed in Table 2. The comparisons are shown in Table 7 as PA-to-General ratios. The ratios for large arrays are as notable as one to tens of thousands. The larger the particle arrays, the more prominent the ratios. Figures 8–11 are almost the same as Figs. 1–4. The only difference is that the numerical results shown in Figs. 8–11 are from the new PA-type codes, while those in Figs. 1–4 are calculated from the general GMM codes. We see that noisy spikes appearing in Figs. 1–4, which are most likely due to random numerical errors, are cleaned up in Figs. 8–11, mainly because a considerable amount of computations are sidestepped, as mentioned earlier.

D. Example Regular Array of 10^8 Identical Spheres

Shown in Table 8 are the total cross sections of a 10001×10001 rectangular array of identical homogeneous spheres,

Table 6. Computer Memory and CPU Time Required for the Scattering Calculations on an 8-Core 2.4 GHz DELL PRECISION T7500 Computer for the Regular Arrays of Identical Particles Listed in Table 1 When Using the New PA-Type of GMM Codes

Array-ID	L1	L2	S1	S2	S3
CPU (min)	0.11	0.12	0.11	0.21	0.73
Memory (Gb)	0.27	0.053	0.27	0.053	0.053

Table 7. Ratios of the CPU and Computer Memory Required in the PA-type GMM Calculations to Those Shown in Table 2

Array-ID	L1	L2	S1	S2	S3
CPU-Ratio	1:350	1:850	1:4100	1:14700	1:71400
Memory-Ratio	1:5	1:4	1:14	1:11	1:39

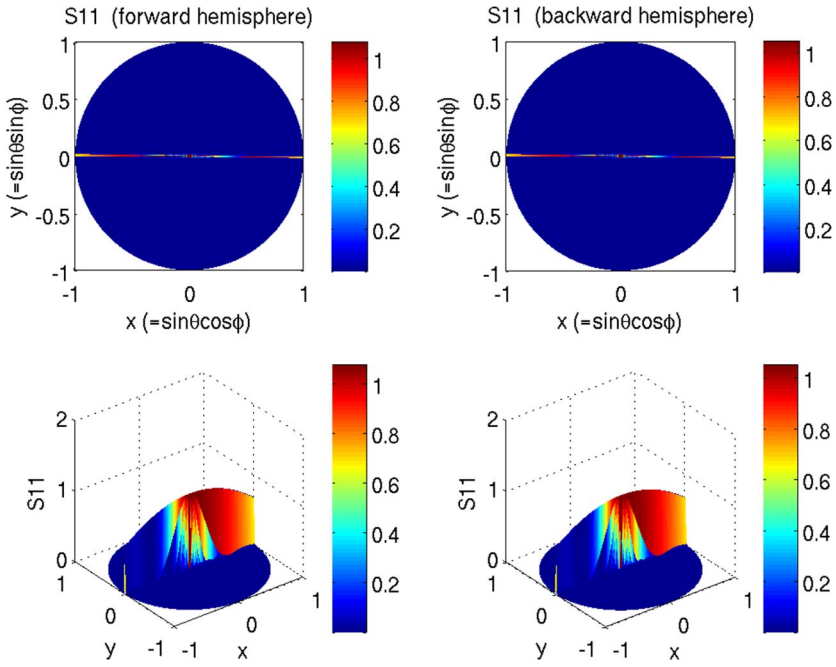

Fig. 8. Same as Fig. 1 except the numerical results shown are obtained from the newly developed "gmm03_PA.f" instead of "gmm03s.f".

calculated from "gmm01_PA.f" for a z propagating, linearly x- or y-polarized plane wave of wavelength 31.416 mm. An individual sphere with a 1 mm diameter has the refractive index of (1.6, 0.1). All sphere centers are on the x–y plane with rows parallel to the x axis and columns parallel to the y axis, equally spaced 1 cm apart in the x direction and 1 mm in the y direction. Spheres are more densely packed in the y direction. Figure 12 shows the spatial distribution of the Stokes parameter Q for the rectangular sphere array when the incident plane wave is unpolarized. The required computer memory is 0.053 Gb, the same as for the linear array L2 and square arrays S2 and S3, independent of the total particle number. The required CPU time is 19.3 minutes, used mostly in the computation of C-type coefficients and the cross sections for radiation pressure.

4. REMARKS AND FUTURE WORK

When applying GMM to PAs, the general scattered-field solution process is radically simplified; only that of a single component particle needs to be solved. The total number of unknowns in the linear system for solving partial scattering coefficients is reduced to its possible minimum. Except for this simplification, all other parts of GMM remain unchanged.

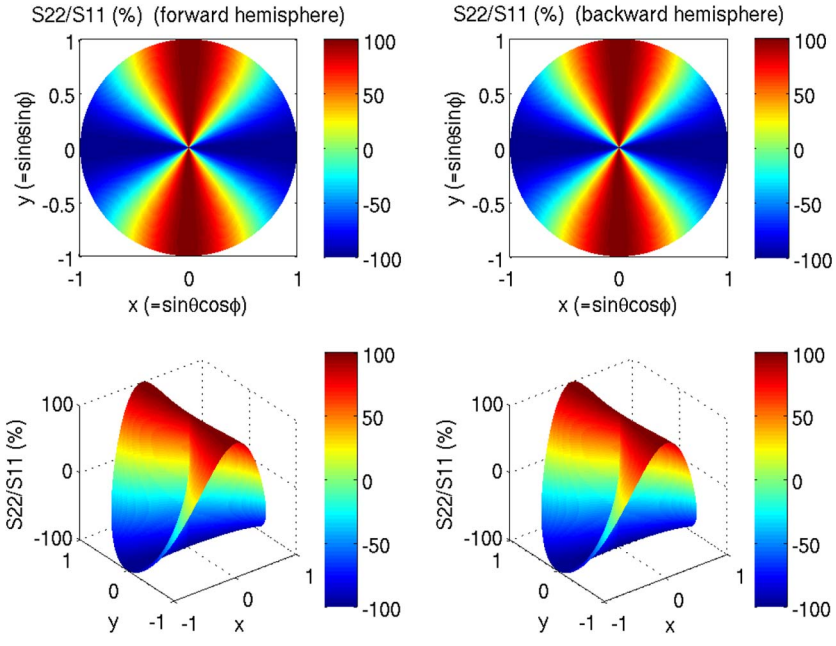

Fig. 9. Same as Fig. 2 except the numerical results shown are obtained from the newly developed "gmm03_PA.f" instead of "gmm03s.f".

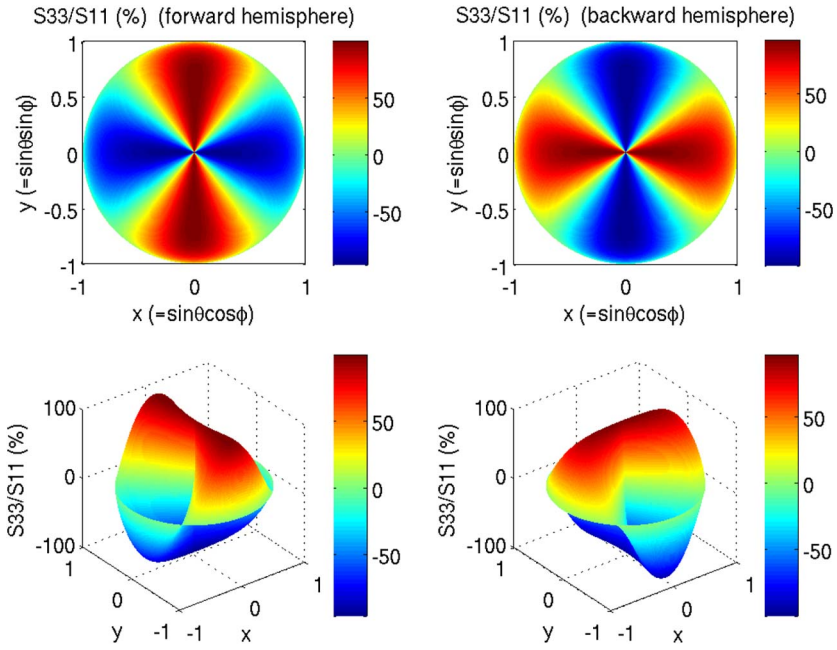

Fig. 10. Same as Fig. 3 except the numerical results shown are obtained from the newly developed "gmm03_PA.f" instead of "gmm03s.f".

The special version of the scattering formulation has been implemented in new PA-type of GMM computer codes for one- and two-dimensional regular arrays of identical particles. This special formulation is derived from periodic structures of infinite dimensions. When applied to particle arrays of finite lengths, the truncation in the spatial periodic structure introduces inevitable truncation errors into numerical results, due to the edge effect. However, practical numerical examples show the special PA-type codes are able to provide numerical solutions with acceptable accuracy when the total number of replica particles is sufficiently large and the edge effect becomes insignificant.

To run the new PA-type codes, the required computer memory only depends on the physical size and shape of an individual particle. Therefore, it stays low, as it is insensitive to the total number of component particles in an array. Similarly, the required computing time will not be intolerable, making it feasible to quickly calculate an array with a huge number of particles, say $\sim 10^8$, which the solution procedure generally used for arbitrary ensembles of scattering bodies cannot presently do. This paves a new way to investigate scattering characteristics of finite periodic structures.

The formulation presented in this work can be extended to three-dimensional PAs. Also, the basis unit in a PA can be of

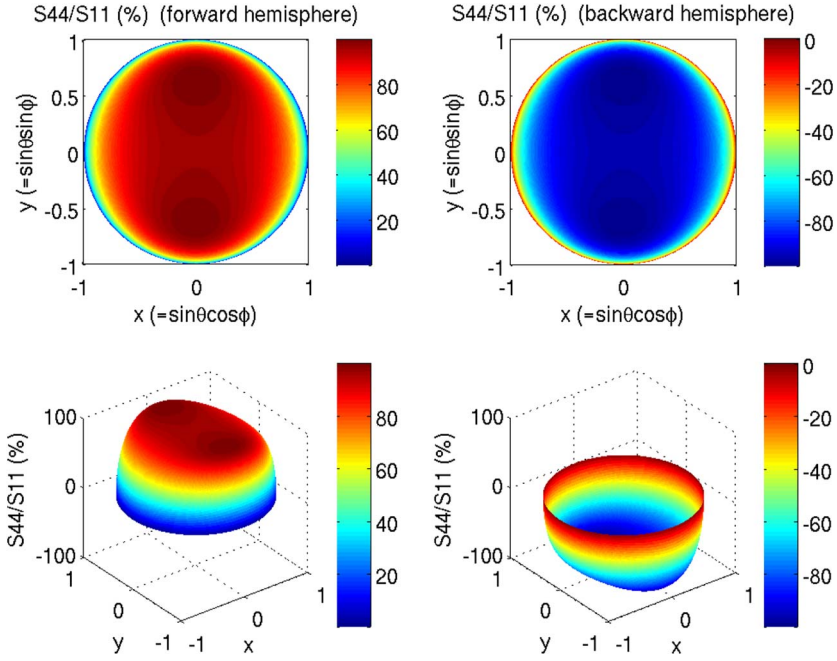

Fig. 11. Same as Fig. 4 except the numerical results shown are obtained from the newly developed "gmm03_PA.f" instead of "gmm03s.f".

Table 8. Total Cross Sections (mm^2) of a 10001 × 10001 Rectangular Array of Identical Homogeneous Spheres Calculated from the Newly Developed GMM Code "gmm01_PA.f"

Incident Polar.	Cext	Cabs	Csca	Cbak	Cpr
x-polarized	1.2635e6	1.2133e6	4.9659e4	3.1229e11	1.2633e6
y-polarized	2.5150e6	2.4171e6	9.7167e4	6.1871e11	2.5146e6

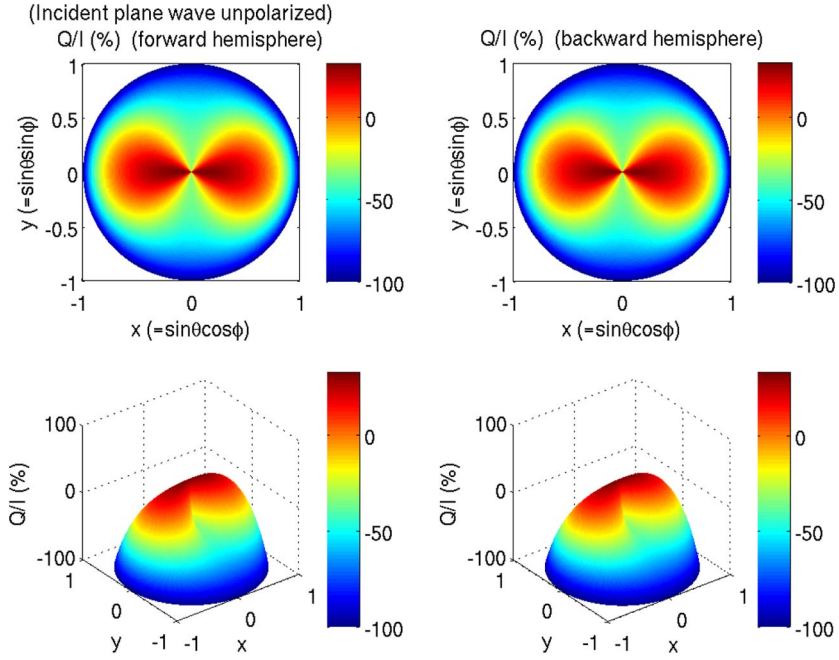

Fig. 12. Dependence of the Stokes parameter Q on scattering angle θ and azimuth angle φ for a 10001 × 10001 rectangular array of identical spheres. The incident plane wave of wavelength 31.416 mm is unpolarized, propagating in the positive z direction. An individual sphere is of refractive index (1.6, 0.1) and of diameter 1 mm. All sphere centers are in the x–y plane with rows parallel to the x axis and columns parallel to the y axis, equally spaced by 10 mm in the x direction and 1 mm in the y direction.

an arbitrarily complex structure itself. The only requirement is that the proper T-matrix of the complex unit cell can be computed with sufficient accuracy.

It would be beneficial to have an efficient way to evaluate the C-coefficients in Eqs. (38) or (39), which are determined only by the geometrical structure of an array. Future research may develop explicit expressions or efficient schemes for evaluating the coefficients in an integrated way, rather than adding each component unit center individually. This will help to improve further the efficiency of the scattering solution process.

Future work may also include a thorough study of the edge effect. The specific approach for PAs provides only approximate numerical solutions to arrays with finite lengths. An extensive investigation of the edge effect will help to determine how large an array must be to ensure a desired accuracy for numerical solutions. The investigation may also be extended to particle arrays with complex boundaries.

REFERENCES

1. P. C. Waterman and N. E. Pedersen, "Electromagnetic scattering by periodic arrays of particles," J. Appl. Phys. **59**, 2609–2618 (1986).
2. I. E. Psarobas and N. Stefanov, "Scattering of elastic waves by periodic arrays of spherical bodies," Phys. Rev. B **62**, 278–291 (2000).
3. A. D. Yaghjian, "Scattering-matrix analysis of linear periodic arrays," IEEE Trans. Antennas Propag. **50**, 1050–1064 (2002).
4. D. A. Genov, A. K. Sarychev, V. M. Shalaev, and A. Wei, "Resonant field enhancements from metal nanoparticle arrays," Nano Lett. **4**, 153–158 (2003).
5. B. T. Draine and P. J. Flatau, "Discrete-dipole approximation for periodic targets: theory and tests," J. Opt. Soc. Am. A **25**, 2693–2703 (2008).
6. F. J. García de Abajo, "Colloquium: light scattering by particle and hole arrays," 2009, http://arXiv.org/pdf/0903.1671.pdf.
7. E. M. Purcell and C. R. Pennypacker, "Scattering and absorption of light by nonspherical dielectric grains,"Astrophys. J. **186**, 705–714 (1973).
8. B. T. Draine, "The discrete-dipole approximation and its application to interstellar graphite grains," Astrophys. J. **333**, 848–872 (1988).
9. B. T. Draine and P. Flatau, "Discrete-dipole approximation for scattering calculations," J. Opt. Soc. Am. A **11**, 1491–1499 (1994).
10. B. Friedman and J. Russek, "Addition theorems for spherical waves," Quart. Appl. Math. **12**, 13–23 (1954).
11. S. Stein, "Addition theorems for spherical wave functions," Quart. Appl. Math. **19**, 15–24 (1967).
12. O. R. Cruzan, "Translational addition theorems for spherical vector wave functions," Quart. Appl. Math. **20**, 33–40 (1962).
13. C. Liang and Y. T. Lo, "Scattering by two spheres," Radio Sci. **2**, 1481–1495 (1967).
14. J. H. Bruning and Y. T. Lo, "Multiple scattering of EM waves by spheres, part I & II," IEEE Trans. Antennas Propag. **AP-19**, 378–400 (1971).

15. Y.-L. Xu, "Electromagnetic scattering by an aggregate of spheres," Appl. Opt. **34**, 4573–4588 (1995).
16. Y.-L. Xu, "Electromagnetic scattering by an aggregate of spheres: far field," Appl. Opt. **36**, 9496–9508 (1997).
17. Y.-L. Xu and R. T. Wang, "Electromagnetic scattering by an aggregate of spheres: theoretical and experimental study of the amplitude scattering matrix," Phys. Rev. E **58**, 3931–3948 (1998).
18. Y.-L. Xu, "Electromagnetic by an aggregate of spheres: asymmetry parameter," Phys. Lett. A **249**, 30–36 (1998).
19. Y.-L. Xu, B. Å. S. Gustafson, F. Giovane, J. Blum, and S. Tehranian, "Calculation of the heat-source function in photophoresis of aggregated spheres," Phys. Rev. E **60**, 2347–2365 (1999).
20. Y.-L. Xu and B. Å. S. Gustafson, "A generalized multiparticle Mie-solution: further experimental verification," J. Quant. Spectrosc. Radiat. Transfer **70**, 395–419 (2001).
21. Y.-L. Xu and N. G. Khlebtsov, "Orientation-averaged radiative properties of an arbitrary configuration of scatterers," J. Quant. Spectrosc. Radiat. Transfer **79–80**, 1121–1137 (2003).
22. Y.-L. Xu, "Radiative scattering properties of an ensemble of variously shaped small particles," Phys. Rev. E **67**, 046620 (2003).
23. Y.-L. Xu, "Scattering Mueller matrix of an ensemble of variously shaped small particles," J. Opt. Soc. Am. A **20**, 2093–2105 (2003).
24. Y.-L. Xu and B. Å. S. Gustafson, "Light scattering by an ensemble of small particles," in *Recent Research Developments in Optics* (Research Signpost, 2003), pp. 599–648.
25. Y.-L. Xu, "Radiative-scattering signatures of an ensemble of nonspherical particles," J. Quant. Spectrosc. Radiat. Transfer **89**, 385–419 (2004).
26. GMM public-domain FORTRAN codes are currently available at http://code.google.com/p/scatterlib.
27. Y.-L. Xu, "Fast evaluation of the Gaunt coefficients," Math. Comput. **65**, 1601–1612 (1996).
28. Y.-L. Xu, "Calculation of the addition coefficients in electromagnetic multisphere-scattering theory," J. Comput. Phys. **127**, 285–298 (1996).
29. Y.-L. Xu, "Calculation of the addition coefficients in electromagnetic multisphere-scattering theory" (erratum), J. Comput. Phys. **134**, 200 (1997).
30. Y.-L. Xu, "Fast evaluation of Gaunt coefficients: recursive approach," J. Comput. Appl. Math. **85**, 53–65 (1997).
31. Y.-L. Xu, "Efficient evaluation of vector translation coefficients in multiparticle light-scattering theories," J. Comput. Phys. **139**, 137–165 (1998).
32. J. A. Gaunt, "On the triplets of helium," Philos. Trans. R. Soc. London Ser. A **228**, 151–196 (1929).
33. E. P. Wigner, "On the matrices which reduce the Kronecker products of representations of simply reducible groups," in *Quantum Theory of Angular Momentum*, L. C. Biedenham and H. van Dam, eds. (Academic, 1965), pp. 89–132.
34. H. A. van der Vorst, "BI-CGSTAB: a fast and smoothly converging variant of BI-CG for the solution of nonsymmetric linear systems," SIAM J. Sci. Stat. Comput. **13**, 631–644 (1992).
35. M. H. Gutknecht, "Variants of BICGSTAB for matrices with complex spectrum," SIAM J. Sci. Comput. **14**, 1020–1033 (1993).
36. H. C. van de Hulst, *Light Scattering by Small Particles* (Wiley, 1957).
37. C. F. Bohren and D. R. Huffman, *Absorption and Scattering of Light by Small Particles* (Wiley, 1983).

57.175.235.23 {ts '2018-03-28 13:00:42'}